

Materials Produced From Plant Biomass. Part II: Evaluation of Crystallinity and Degradation Kinetics of Cellulose

Matheus Poletto^{a,b*}, Vinícios Pistor^c, Ruth Marlene Campomanes Santana^a, Ademir José Zattera^b

^aEngineering School, Federal University of Rio Grande do Sul – UFRGS, Porto Alegre, RS, Brazil

^bLaboratory of Polymers – LPOL, Center of Exact Sciences and Technology – CCET, Caxias do Sul University – UCS, Caxias do Sul, RS, Brazil

^cChemical Institute, Federal University of Rio Grande do Sul – UFRGS, Porto Alegre, RS, Brazil

Received: December 9, 2011; Revised: February 26, 2012

In this study *Eucalyptus grandis* (CEG) and *Pinus taeda* (CPT) cellulose fibers obtained from kraft and sulfite pulping process, respectively, were characterized using Fourier transform infrared (FTIR) spectroscopy and thermogravimetry (TGA). The degradation kinetic parameters were determined by TGA using Coats and Redfern method. FTIR results showed that CPT presented a more ordered structure with higher crystallinity than CEG. Thermogravimetric results showed that CPT had a higher thermal stability than CEG. The kinetic results reveal that for CEG the degradation mechanism occurs mainly by random nucleation, although phase boundary controlled reactions also occurs while for CPT the degradation process is more related with phase boundary controlled reactions. Results demonstrated that differences between thermal stability and degradation mechanisms might be associated with differences in the cellulose crystalline structure probably caused by different pulping processes used for obtaining the cellulose fibers.

Keywords: *Eucalyptus grandis*, *Pinus taeda*, cellulose, crystallinity, FTIR spectroscopy, thermal degradation

1. Introduction

Cellulose fibers are extensively used to reinforce polymeric composite materials¹⁻⁴. The considerable interest in these fibers is due to their biodegradability, renewability, low density and mechanical properties comparable to those inorganic fibers⁵. Cellulose is a natural polymer consisting of D-anhydroglucose (C₆H₁₁O₅) repeating units joined by 1,4-β-D-glycosidic linkages at C1 and C4 position⁶. Each repeating unit contains three hydroxyl groups. These hydroxyl groups and their ability to hydrogen bond play a major role in directing the crystalline packing and also govern the physical properties of cellulose⁶. Solid cellulose forms a microcrystalline structure with regions of highly order i.e. crystalline regions and low order regions i.e. amorphous regions.

In native cellulose, the crystalline regions are cellulose I, which consists of two allomorphous phases. The cellulose Iβ, characterized by a monoclinic unit cell with two polymer chains in a parallel arrangement, and cellulose Iα, with a shift of the polymer chains along the chain axis, resulting in a triclinic unit cell^{7,8}. The relative amounts of phases Iα and Iβ depend on the origin and the chemical treatment of the cellulose.

Changes in cellulose fibers and their aggregates occurring during pulping process and have impact on the fiber properties and crystallinity that are important factors when cellulose was used in composite formulations. Hult et al.⁹ investigated the hierarchic organization of cellulose

microfibrils in kraft and sulfite pulp fibers and showed that the kraft fibers exhibit higher ordered cellulose regions and more aggregated fibrils in contrast to the sulfite fibers. This may contribute to higher crystallinity in kraft fibers. However, pulping conditions as cooking temperature may influence on cellulose properties. The increase in cooking temperature during pulping process can promote more chain scission reactions increasing the amorphous character of the cellulose, which reduce the total amount of cellulose crystalline regions^{9,23}.

Cellulose crystallinity is one of the most important crystalline structure parameters in cellulose fibers¹⁰. The thermal stability of cellulose was found to depend mainly on its crystallinity^{11,12}. Thus, cellulose crystallinity and hydrogen bond between cellulose chains play an important role in the mechanical and thermal properties of composite materials reinforced with cellulose fibers^{1,13}. Several techniques as X-ray diffraction and FTIR spectroscopy were used to evaluate the wood and cellulose crystallinity^{5,7,8,9,10,12}. However, FTIR spectroscopy has been used as a simple technique for obtaining rapid information about the structure of cellulose and chemical changes taking place in cellulose due to various treatments^{10,21,22,25-27}.

As mentioned earlier, the crystalline structure of cellulose affects the physical, mechanical and thermal properties of cellulose fibers. Thus, it is paramount to ascertain the structure of cellulose and its crystallinity whenever cellulose fibers are intended for use as a reinforcing

*e-mail: mpolett1@ucs.br

agent in composite materials. The aim of this study was to investigate the differences between two cellulose samples resulting from two different pulping processes and evaluate how these differences influence the thermal properties and decomposition kinetics of the cellulose fibers analyzed.

2. Material and Methods

2.1. Materials

Bleached sulfite cellulose fibers from *Pinus taeda* (CPT) were supplied by Cambará S.A. (Cambará do Sul, Brazil) obtained at cooking temperature of 140 °C and bleaching with hydrogen peroxide. Bleached kraft cellulose fibers from *Eucalyptus grandis* (CEG) were supplied by CMPC S.A. (Guaíba, Brazil), obtained at cooking temperature of 155 °C, bleaching with hydrogen peroxide. The samples were dried at 70 °C for 24 hours in a vacuum oven before the tests. The average fiber particle length for CTP and CEG is around 150 µm.

2.2. Fourier transform infrared (ftir) spectroscopy

Fourier transform infrared spectroscopy spectra were obtained using a spectrometer Nicolet IS10- Thermo Scientific. Samples of the finely divided celluloses (5 mg) were dispersed in a matrix of KBr (100 mg) followed by compression to form pellets. The sample collection was obtained using 32 scans, from 4000 to 400 cm⁻¹, at a resolution of 4 cm⁻¹. Care was taken to ensure all samples remained dry during sample preparation and FTIR analysis.

2.3. Thermogravimetric analysis (TGA)

Thermogravimetric analysis (TGA50-Shimadzu) was carried out under N₂ atmosphere, from 25 up to 610 °C. Approximately 10 mg of each sample was used. The analysis was carried out at four different heating rates (5, 10, 20 and 40 °C/min). The results obtained were used to calculate the kinetics parameters.

2.4. Theoretical consideration

2.4.1. Coats and redfern method

The conversion rate (α) is defined according to Equation (1)^{12,14,15} as:

$$\alpha = \frac{m_0 - m_i}{m_0 - m_f} \quad (1)$$

where m_0 , m_f and m_i are the initial and final weights of the sample and its weight at temperature (T), respectively. For determining the degradation kinetic mechanism, the reactions are considered irreversible and the reaction rate is both dependent of the activation energy and reaction order¹⁶. These parameters can be estimated by combining the Arrhenius equation with non-isothermal experiments using the relationship described in Equation (2):

$$\frac{d\alpha}{dt} = f(\alpha) A \exp\left(-\frac{E_a}{RT}\right) \quad (2)$$

where $f(\alpha)$, A , E_a , R and T are the reaction model, pre-exponential factor, activation energy, universal gas constant (8.314 J.mol⁻¹ K) and temperature (in Kelvin), respectively. The Coats and Redfern method¹⁷ is not based on derivatives of $d\alpha/dt$. However, in the non-isothermal method the temperature increases linearly, the time (t) variable is eliminated and the Equation (2) can be rewritten as¹⁸:

$$\frac{d\alpha}{f(\alpha)} = \frac{A \exp\left(-\frac{E_a}{RT}\right)}{\beta} \times \exp\left(-\frac{E_a}{RT}\right) dT \quad (3)$$

where, β is the heating rate. As the term $\exp(-E_a/RT)$ does not have exact solution the Taylor expansion is used^{17,18}. After integration of Equation (3) the Equation (4) can be obtained:

$$\int_0^\alpha \frac{d\alpha}{f(\alpha)} = g(\alpha) - g(0) = \frac{A \exp\left(-\frac{E_a}{RT}\right) R}{\beta E_a} T^2 \left(1 - \frac{2RT}{E_a}\right) \exp\left(-\frac{E_a}{RT}\right) \Bigg|_{T_0}^T \quad (4)$$

Considering the possible degradation mechanisms in solid state reactions, the solution for Coats and Redfern Equation can be obtained replacing the function $g(\alpha)$ by the mechanisms described in Table 1^{116,18}. When the values of n were different from one, the method can be described by Equation (5) and when the values of n were equal to one the Equation (4) is summarized by Equation (6)¹⁷:

$$\log\left(\frac{1-(1-\alpha)^{1-n}}{T^2(1-n)}\right) = \log\frac{AR}{\beta E_a} \left(1 - \frac{2RT}{E_a}\right) - \frac{E_a}{2.3RT} n \neq 1 \quad (5)$$

$$\log\left(-\frac{\log(1-\alpha)}{T^2}\right) = \log\frac{AR}{\beta E_a} \left(1 - \frac{2RT}{E_a}\right) - \frac{E_a}{2.3RT} n = 1 \quad (6)$$

Therefore, to evaluate which degradation mechanism is closer to the solid state reaction under study, it is possible to replace the values of the functions showed in Table 1 by isolating the term on the left side of Equation (5) or Equation (6) as a function of inverse temperature (1/T).

The plot of $\log\left(\frac{1-(1-\alpha)^{1-n}}{T^2(1-n)}\right)$ against 1/T should result in a straight line with a slope of $(-E_a/2.3R)$. In fact, the calculations have to be performed using several values of n in order to retain the value leading to the best linear relationship.

3. Results and Discussions

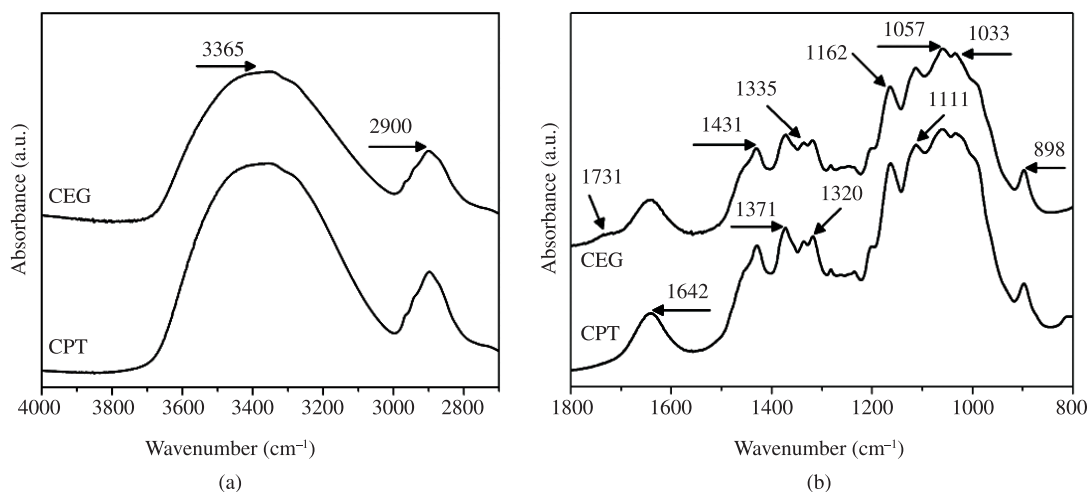
3.1. Fourier transform infrared (ftir) spectroscopy

FTIR spectroscopy has been used as a simple technique for obtaining rapid information about the chemical structure and crystallinity of celluloses samples^{5,19}. Contrary to conventional chemical analysis, this method requires small sample sizes, short analysis time besides being non-destructive²⁰.

Because of their complexity, the spectra were separated into two regions, namely: the OH and CH stretching vibrations in the 4000-2700 cm⁻¹ region, showed in Figure 1a, and the "fingerprint" region which is assigned to different stretching vibrations of different groups in 1800-800 cm⁻¹, Figure 1b. It can be observed in Figure 1a

Table 1. Algebraic expressions commonly used for solid thermal decomposition processes.

Mechanism - Solid state process	$g(\alpha)$	$f(\alpha)$
$A_{(n)}$ - Nucleation and growth	$[-\ln(1-\alpha)]^{1/n}$	$n(1-\alpha)[- \ln(1-\alpha)]^{(n-1)/n}$
R_2 - Phase boundary controlled reaction (contracting area)	$[1-\ln(1-\alpha)^2]^{1/2}$	$2(1-\alpha)^{1/2}$
R_3 - Phase boundary controlled reaction (contracting volume)	$[1-\ln(1-\alpha)^3]^{1/3}$	$3(1-\alpha)^{2/3}$
D_1 - One-dimensional diffusion	α^2	$(1/2)\alpha^{-1}$
D_2 - Two-dimensional diffusion (Valensi equation)	$(1-\alpha)\ln(1-\alpha)+\alpha$	$-[\ln(1-\alpha)]^{-1}$
D_3 - Three-dimensional diffusion (Jander equation)	$[1-(1-\alpha)^3]^{1/2}$	$(3/2)[1-(1-\alpha)^2]^{-1/2}(1-\alpha)^{3/2}$
D_4 - Three-dimensional diffusion (Ginstling-Brounshtein equation)	$[1-(2/3)\alpha]-(1-\alpha)^{2/3}$	$(3/2)[1-(1-\alpha)^{1/3}]^{-1}$
F_1 - Random nucleation with one nucleus on the individual particle	$-\ln(1-\alpha)$	$1-\alpha$

**Figure 1.** FTIR spectra of celluloses studied in the region between 4000-2800 cm^{-1} (a) and between 1800-800 cm^{-1} (b).

a strong broad band in the region of 3700-3000 cm^{-1} which is assigned to different OH stretching modes and another band in the region of 3000-2800 cm^{-1} is ascribed to the stretching of asymmetric and symmetric methyl and methylene CH cellulose groups¹⁹. The band at around 3360 cm^{-1} related with OH stretching modes is more prominent for CPT than for CEG. This is probably due to a larger number of hydroxyl groups in CPT which may be associated with an increase in the number of hydrogen bonds formed. Thus, a mixture of intermolecular and intramolecular hydrogen bonds is considered to cause the broadening of the OH band in the IR spectra²⁰.

Figure 1b shows that in the “fingerprint” region the spectra revealed several bands. The band at 1642 cm^{-1} is associated with adsorbed water in cellulose^{19,22,23}. The bands at 1430, 1370, 1335 and 1320 cm^{-1} are attributed to CH_2 symmetric bending, CH bending, OH in plane bending, CH_2 rocking vibration, respectively²¹⁻²³, and the bands at 1162, 1111,

1057, 1033, 898 cm^{-1} are assigned to asymmetric C-O-C bridge stretching, the anhydroglucose ring asymmetric stretching, C-O stretching, C-H in plane deformation, C-H deformation of cellulose, respectively^{21-24,26}. On the other hand, the peaks for xylan from hemicelluloses are derived from molecular vibrations in the uronic acids at 1730 and 1600 cm^{-1} ¹²⁸¹. CEG sample showed a more prominent peak than CPT at around 1730 cm^{-1} while the band at 1600 cm^{-1} overlap with the band at 1642 cm^{-1} associated with adsorbed water in cellulose^{19,22,23}. This may indicate that xylan is more alkali resistant and probably hemicelluloses can be precipitation on the surface of the eucalyptus cellulose fibers during kraft cooking^{28,29}.

The ratio between the heights of the bands at 1372 and 2900 cm^{-1} proposed by Nelson and O'Connor (1964) as total crystalline index (TCI)²² was used to evaluate the infrared (IR) crystallinity ratio. The band at 1430 cm^{-1} is associated with the amount of crystalline structure of

cellulose, while the band at 898 cm^{-1} is assigned with the amorphous region in cellulose²⁵. The ratio between the areas of the bands at 1429 and 897 cm^{-1} are used as a lateral order index (LOI)²². Considering the chain mobility and bond distance, the hydrogen bond intensity (HBI) of cellulose is closely related to the crystal system and the degree of intermolecular regularity, that is, crystallinity²⁷. The ratio of the absorbance bands at 3400 and 1320 cm^{-1} was used to study the cellulose samples HBI. The obtained results are displayed in Table 2.

The TCI is proportional to the crystallinity degree of cellulose²⁰ and LOI is correlated to the overall degree of order in cellulose^{22,26}. Based on this fact, the CPT showed the highest TCI and LOI value indicating highest degree of crystallinity and more ordered cellulose structure than the CEG. On the other hand, CEG presented lowest TCI and LOI value which may indicate that this cellulose is composed for more amorphous domains in the cellulose structure when compared with the CPT. The HBI value is higher for CPT than for CEG sample. This result might be indicated that CPT contain much more cellulose chains in a highly organized form which can lead to higher hydrogen bond intensity between neighbor cellulose chains and result in more packing cellulose structure and higher crystallinity than CEG. The crystallinity of cellulose is closed related with the thermal stability^{12,30}. Therefore, it is possible that cellulose samples with highest TCI, LOI and HBI may exhibit higher thermal stability.

3.2. Thermogravimetric analysis

Figure 2 shows the TGA and derivative thermogravimetric (DTG) curves of the cellulose samples studied. A small weight loss for both samples occurs between 40 - $70\text{ }^{\circ}\text{C}$ which is attributed to the removal of absorbed water in cellulose^{14,31}.

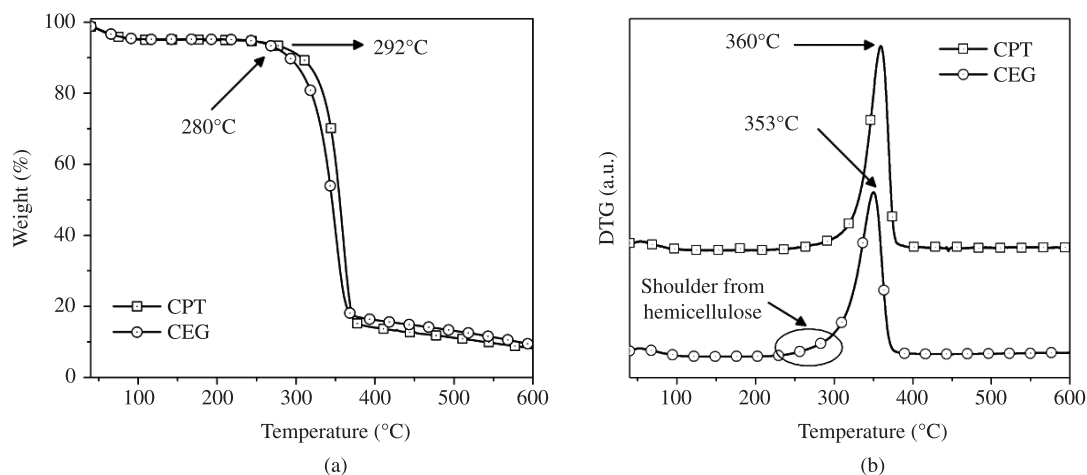


Figure 2. TGA (a) and DTG (b) curves of the cellulose samples studied.

Table 2. Cellulose infrared crystallinity ratios and hydrogen bond intensity

Cellulose samples	IR crystallinity ratio		HBI A3400/A1320
	H1372/H2900 (TCI)	A1429/A897 (LOI)	
CEG	0.457 ± 0.020	3.507 ± 0.344	1.368 ± 0.014
CPT	0.491 ± 0.010	4.071 ± 0.128	1.455 ± 0.002

As depicted in Figure 2a, the CEG sample initiates a more pronounced degradation process at around $280\text{ }^{\circ}\text{C}$ while for CPT a more pronounced degradation process occurs at $292\text{ }^{\circ}\text{C}$. At this reaction time, the cleavage of the glycosidic linkages of cellulose reduces the polymerization degree leading to the formation of organic compounds like alkenes and other hydrocarbon derivatives^{32,33} and after $400\text{ }^{\circ}\text{C}$ the residual decomposition process can lead to formation of CO , CO_2 , H_2O and char^{5,31}. The DTG curve of CPT was shifted to higher temperatures than CEG. The DTG peak occurs at $353\text{ }^{\circ}\text{C}$ for CEG and $360\text{ }^{\circ}\text{C}$ for CPT, as shown in Figure 2b. This result suggests that celluloses with higher TCI, LOI and HBI have higher thermal stability probably due to the much more hydrogen bonds between cellulose chains that can result in more ordered and packing cellulose regions, this in turn possibly increasing the thermal decomposition temperature of cellulose. Moreover, the CEG sample presented a small shoulder between 250 and $300\text{ }^{\circ}\text{C}$. This behaviour can be associated with the hemicellulose degradation in this sample. According Yang et al.³¹ hemicellulose starts a more prominent decomposition between 220 - $315\text{ }^{\circ}\text{C}$. However, for both CEG and CPT samples the start of hemicellulose decomposition is difficult to distinguish and overlaps with the degradation of cellulose.

3.3. Kinetics results

Figure 3 illustrates the application of the Coats and Redfern method for the kinetic models listed in Table 1. The values of n used were 3.42 and 2.45 for CEG and CPT, respectively according to a previous work¹². As can be seen in Figure 3a, the best fits using the Coats and Redfern method for CEG indicated that for this cellulose sample the degradation process occurs by first order reaction with random nucleation resulting in an F1 mechanism, which is

in agreement with the results describes by Conesa et al.³⁸ and Dahiya et al.³⁹. On the other hand, phase boundary controlled reactions with contracting area and contracting volume also occurs, in agreement with other results from the literature³³⁻³⁷. This degradation behavior may be associated with the lower crystallinity of the CEG sample observed by FTIR results. The degradation process probably starts sporadically on the cellulose amorphous domains from the entire sample. When the crystalline domains degradation takes place the degradation initially occurs on the crystallites surface and phase boundary controlled reactions also described the degradation mechanism. For the CPT sample the best fit occurs by a degradation mechanism corresponded to R_n , i.e. the phase boundary-controlled reaction, as shown in Figure 3b. Similar results were described by Wu and Dollimore³⁴. Once again, the FTIR results may be explained better the degradation mechanism. The CPT sample had higher crystallinity than CEG, as can be seen in Table 2. The more packing cellulose chains in CPT sample might be difficult the heat transfer by diffusion through the cellulose chains and then the degradation process may be initially occurs by degradation of the surface of the cellulose crystallites with contraction of the area and volume, resulting in R2 and R3 degradation mechanisms.

The activation energy values for CEG were found in the range of 173-190 $\text{kJ}\cdot\text{mol}^{-1}$ and for CPT between 124-126 $\text{kJ}\cdot\text{mol}^{-1}$, as presented in Table 3. The values found for both cellulose samples are consistent with the values reported in the literature^{38,39}. However, the CEG sample had a higher activation energy range than the CPT sample.

The lower activation energy values observed for CPT might be attributed to the thermal decomposition of this sample being controlled by dehydration which results in anhydrocellulose. The CPT sample showed a higher band at 1642 cm^{-1} assigned to the adsorbed water into the cellulose structure, see Figure 1b. The more quantity of adsorbed water into the cellulose structure of CPT sample may be responsible for initiate the degradation process by dehydration which probably results in lower activation energy values. The higher activation energy for CEG may be indicating that the thermal decomposition occurs by depolymerization of cellulose with production of levoglucosan, according to the classic model proposed by Broido-Shafizadeh^{18,40} as shown in Figure 4. Therefore, the two parallel or competitive reactions occurs for the two cellulose samples study, however dehydration reactions are more prominent for CPT sample while for CEG

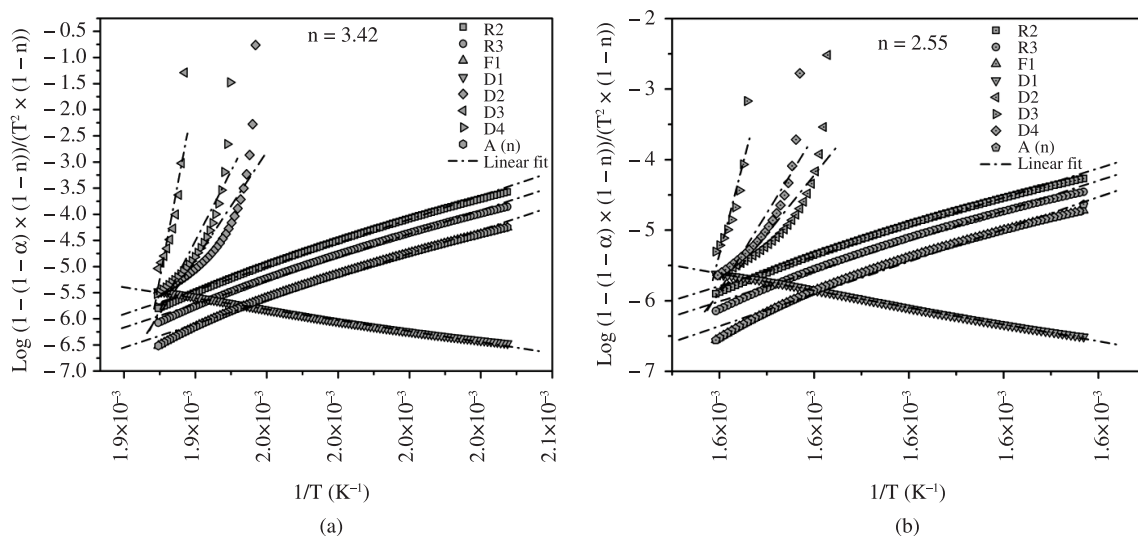


Figure 3. Linear fits of the Coats and Redfern method using different degradation mechanism ($g(\alpha)$) determined through the thermogravimetric curves for $\beta = 10\text{ }^\circ\text{C}/\text{min}$ where: (a) CEG e (b) CPT samples.

Table 3. Activation energy values from Coats and Redfern method

Mechanism	CEG $n = 3.42$		CPT $n = 2.45$	
	E_a ($\text{kJ}\cdot\text{mol}^{-1}$)	r	E_a ($\text{kJ}\cdot\text{mol}^{-1}$)	r
R2	173.37	0.9966	125.65	0.9974
R3	177.90	0.9954	124.24	0.9969
F1	190.00	0.9920	124.64	0.9948
D1	-99.68	-0.9994	-58.17	-0.9973
D2	695.64	0.8940	572.96	0.8807
D3	2150.50	0.9248	1993.65	0.8941
D4	911.53	0.9053	740.26	0.9029
A(n)	190.31	0.9922	124.79	0.9962

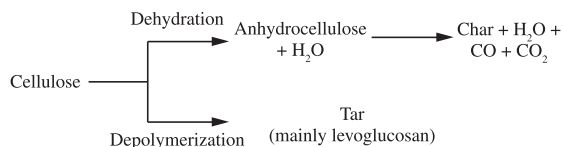


Figure 4. Broido-Shafizadeh reaction scheme for pyrolysis of cellulose^{16,34}.

depolymerization reactions are more predominant. Similar behavior was observed by Soares et al.⁴⁰ for cellulose powder and kraft paper and by Scheirs et al.⁴¹ for cellulose paper and kraft insulating paper.

4. Conclusions

The crystallinity and kinetic decomposition of two cellulose samples obtained by two pulping process were investigated. FTIR results indicated that CPT contains more cellulose chains in a highly organized form which may result in more packing cellulose structure and higher crystallinity than CEG. Thermogravimetric results confirm that CPT sample presented higher thermal stability than CEG probably due to the more ordered cellulose regions.

Through the kinetic parameters it was found that there are differences between the degradation processes

of the cellulose fibers studied. For the CEG sample the degradation processes occurs by random nucleation and probably starts on the cellulose amorphous domains while for CPT, that had more crystallinity regions than CEG, the more packing cellulose chains might be difficult the heat transfer by diffusion through the cellulose chains and then the degradation process may be occurs by degradation of the surface of the cellulose crystallites with a phase boundary controlled reaction.

The lower activation energy values observed for CPT than CEG might be attributed to the thermal decomposition of this sample being controlled by dehydration while for CEG the higher activation energy values probably indicated that the thermal decomposition occurs by depolymerization of cellulose. In general, the crystallinity and thermal stability were more affected by the kraft pulping conditions than by those of sulfite pulping. This behavior may be associated with the higher cooking temperature used during the cooking process employed for the CEG sample.

Acknowledgments

The authors acknowledge Cambará S.A., CMPC S.A. for supplying the cellulose fibers and CAPES for a fellowship.

References

- Bengtsson M, Le Baillif M and Oksman K. Extrusion and mechanical properties of highly filled cellulose fibre-polypropylene composites. *Composites Part A*. 2007; 38:1922-1931. <http://dx.doi.org/10.1016/j.compositesa.2007.03.004>
- Qiu W, Zhang F, Endo T and Hirotsu T. Preparation and characterization of composites of high-crystalline cellulose with polypropylene: effects of maleated polypropylene and cellulose content. *Journal of Applied Polymer Science*. 2003; 87:337-345. <http://dx.doi.org/10.1002/app.11446>
- Borja Y, Rieb G and Lederer K. Synthesis and characterization of polypropylene reinforced with cellulose I and II fibers. *Journal of Applied Polymer Science*. 2006; 101:364-369. <http://dx.doi.org/10.1002/app.23847>
- Spoljaric S, Genovese A and Shanks RA. Polypropylene-microcrystalline cellulose composites with enhanced compatibility and properties. *Composites Part A*. 2009; 40:791-799. <http://dx.doi.org/10.1016/j.compositesa.2009.03.011>
- Quiévy N, Jacquet N, Sclavons M, Deroanne C, Paquot M and Devaux J. Influence of homogenization and drying on the thermal stability of microfibrillated cellulose. *Polymer Degradation and Stability*. 2010; 95:306-314. <http://dx.doi.org/10.1016/j.polymdegradstab.2009.11.020>
- John MJ and Thomas S. Biofibres and biocomposites. *Carbohydrate Polymers*. 2008; 71:343-364. <http://dx.doi.org/10.1016/j.carbpol.2007.05.040>
- Newman RH. Estimation of the lateral dimensions of cellulose crystallites using ¹³C NMR signal strengths. *Solid State Nuclear Magnetic Resonance*. 1999; 15:21-29. [http://dx.doi.org/10.1016/S0926-2040\(99\)00043-0](http://dx.doi.org/10.1016/S0926-2040(99)00043-0)
- Wada M and Okano T. Localization of I α and I β phases in algal cellulose revealed by acid treatments. *Cellulose*. 2001; 8:183-188. <http://dx.doi.org/10.1023/A:1013196220602>
- Hult E-L, Iversen T and Sugiyama J. Characterization of the supermolecular structure of cellulose in wood pulp fibers. *Cellulose*. 2003; 10:103-110. <http://dx.doi.org/10.1023/A:1024080700873>
- Gümüşkaya E, Usta M and Kirei H. The effects of various pulping conditions on crystalline structure of cellulose in cotton linters. *Polymer Degradation and Stability*. 2003; 81:559-564. [http://dx.doi.org/10.1016/S0141-3910\(03\)00157-5](http://dx.doi.org/10.1016/S0141-3910(03)00157-5)
- Nada A-AM.A, Kamel S and El-Sakhawy M. Thermal behaviour and infrared spectroscopy of cellulose carbamates. *Polymer Degradation and Stability*. 2000; 70:347-355. [http://dx.doi.org/10.1016/S0141-3910\(00\)00119-1](http://dx.doi.org/10.1016/S0141-3910(00)00119-1)
- Poletto M, Pistor V, Zeni M and Zattera AJ. Crystalline properties and decomposition kinetics of cellulose fibers in wood pulp obtained by two pulping process. *Polymer Degradation and Stability*. 2011; 96:679-685. <http://dx.doi.org/10.1016/j.polymdegradstab.2010.12.007>
- Neagu RC, Gamstedt EK and Berthold F. Stiffness contribution of various wood fibers to composite materials. *Journal of Composite Materials*. 2006; 40:663-699. <http://dx.doi.org/10.1177/0021998305055276>
- Poletto M, Dettenborn J, Pistor V, Zeni M and Zattera AJ. Materials produced from plant biomass. Part I: evaluation of thermal stability and pyrolysis of wood. *Materials Research*. 2010; 13:375-379. <http://dx.doi.org/10.1590/S1516-14392010000300016>
- Pistor V, Ornaghi FG, Fiorio R and Zattera AJ. Thermal characterization of oil extracted from ethylene-propylene-diene terpolymer residues (EPDM). *Thermochemica Acta*. 2010; 510:93-96. <http://dx.doi.org/10.1016/j.tca.2010.06.028>
- Carmen Albano EF. Thermogravimetric evaluation of the kinetics of decomposition of polyolefin blends. *Polymer*

- Degradation and Stability*. 1998; 61:289-295. [http://dx.doi.org/10.1016/S0141-3910\(97\)00211-5](http://dx.doi.org/10.1016/S0141-3910(97)00211-5)
17. Coats AW and Redfern JP. Kinetic Parameters from Thermogravimetric Data. *Nature*. 1964; 201:68-69. <http://dx.doi.org/10.1038/201068a0>
 18. Capart R, Khezami L and Burnham AK. Assessment of various kinetic models for the pyrolysis of a microgranular cellulose. *Thermochimica Acta*. 2004; 417:79-89. <http://dx.doi.org/10.1016/j.tca.2004.01.029>
 19. Adel MA, Abb El-Wahab ZH, Ibrahim AA and Al-Shemy MT. Characterization of microcrystalline cellulose prepared from lignocellulosic materials. Part II: physicochemical properties. *Carbohydrate Polymers*. 2011; 83:676-687. <http://dx.doi.org/10.1016/j.carbpol.2010.08.039>
 20. Popescu M-C, Popescu C-M, Lisa G and Sakata Y. Evaluation of morphological and chemical aspects of different wood species by spectroscopy and thermal methods. *Journal of Molecular Structure*. 2011; 988:65-72. <http://dx.doi.org/10.1016/j.molstruc.2010.12.004>
 21. Chen H, Ferrari C, Angiuli M, Yao J, Raspi C and Bramanti E. Qualitative and quantitative analysis of wood samples by Fourier transform infrared spectroscopy and multivariate analysis. *Carbohydrate Polymers*. 2010; 82:772-778. <http://dx.doi.org/10.1016/j.carbpol.2010.05.052>
 22. Carrilo F, Colom X, Suñol JJ and Saurina J. Structural FTIR analysis and thermal characterization of lyocell and viscose-type fibres. *European Polymer Journal*. 2004; 40:2229-2234. <http://dx.doi.org/10.1016/j.eurpolymj.2004.05.003>
 23. Schwanninger M, Rodrigues JC, Pereira H and Hinterstoisser B. Effects of short vibratory ball milling on the shape of FT-IR spectra of wood and cellulose. *Vibrational Spectroscopy*. 2004. 36:23-40. <http://dx.doi.org/10.1016/j.vibspec.2004.02.003>
 24. Tserki V, Matzinos P, Kokkou S and Panayiotou C. Novel biodegradable composites based on treated lignocellulosic waste flour as filler. Part I. Surface chemical modification and characterization of waste flour. *Composites Part A*. 2005; 36:965-974. <http://dx.doi.org/10.1016/j.compositesa.2004.11.010>
 25. Åkerholm M, Hinterstoisser B and Salmén L. Characterization of the crystalline structure of cellulose using static and dynamic FT-IR spectroscopy. *Carbohydrate Research*. 2004; 339:569-578. PMID:15013393. <http://dx.doi.org/10.1016/j.carres.2003.11.012>
 26. Corgié SC, Smith HM and Walker LP. Enzymatic transformations of cellulose assessed by quantitative high-throughput Fourier transform infrared spectroscopy (QHT-FTIR). *Biotechnology and Bioengineering*. 2011; 108:1509-1520. PMID:21337332. <http://dx.doi.org/10.1002/bit.23098>
 27. Oh SY, Yoo DI, Shin Y and Seo G. FTIR analysis of cellulose treated with sodium hydroxide and carbon dioxide. *Carbohydrate Research*. 2005; 340:417-428. PMID:15680597. <http://dx.doi.org/10.1016/j.carres.2004.11.027>
 28. Åkerholm M and Salmén L. Dynamic FTIR spectroscopy for carbohydrate analysis of wood pulps. *Journal of Pulp and Paper Science*. 2002; 28:245-249.
 29. Petra Wollboldt R, Zuckerstätter G, Weber HK, Larsson PT and Sixta H. Accessibility, reactivity and supramolecular structure of *E. globulus* pulps with reduced xylan content. *Wood Science and Technology*. 2010; 44:533-546. <http://dx.doi.org/10.1007/s00226-010-0370-2>
 30. Kim U-J, Eom SH and Wada M. Thermal decomposition of native cellulose: influence on crystallite size. *Polymer Degradation and Stability*. 2010; 95:778-781. <http://dx.doi.org/10.1016/j.polymdegradstab.2010.02.009>
 31. Yang H, Yan R, Chen H, Zheng C, Lee DH and Liang DT. In-depth investigation of biomass pyrolysis based on three major components: hemicellulose, cellulose and lignin. *Energy & Fuels*. 2006; 20:388-393. <http://dx.doi.org/10.1021/ef0580117>
 32. Spinacé MAS, Lambert CS, Feroselli KKG and De Paoli M-A. Characterization of lignocellulosic curaua fibres. *Carbohydrate Polymers*. 2009; 77:47-53. <http://dx.doi.org/10.1016/j.carbpol.2008.12.005>
 33. Elanthikkal S, Gopalakrishnapanicker U, Varghese S and Guthrie JT. Cellulose microfibrils produced from banana plant wastes: Isolation and characterization. *Carbohydrate Polymers*. 2010; 80:852-859. <http://dx.doi.org/10.1016/j.carbpol.2009.12.043>
 34. Wu Y and Dollimore D. Kinetic studies of thermal degradation of natural cellulosic materials. *Thermochimica Acta*. 1998; 324:49-57. [http://dx.doi.org/10.1016/S0040-6031\(98\)00522-X](http://dx.doi.org/10.1016/S0040-6031(98)00522-X)
 35. Lerdkanchanaporn S, Dollimore D and Alexander KS. A simultaneous TG-DTA study of the degradation in nitrogen of cellulose to carbon, alone and in the presence of other pharmaceutical excipients. *Thermochimica Acta*. 1998; 324:25-32. [http://dx.doi.org/10.1016/S0040-6031\(98\)00520-6](http://dx.doi.org/10.1016/S0040-6031(98)00520-6)
 36. Bianchi O, Dal Castel C, De Oliveira RVB, Bertuoli P and Hillig E. Avaliação da degradação não-isotérmica de madeira através de termogravimetria-TGA. *Polímeros*. 2010; 20:395-400. <http://dx.doi.org/10.1590/S0104-14282010005000060>
 37. Bourbigot S, Chlebicki S and Mamleev V. Thermal degradation of cotton under linear heating. *Polymer Degradation and Stability*. 2002; 78:57-62. [http://dx.doi.org/10.1016/S0141-3910\(02\)00119-2](http://dx.doi.org/10.1016/S0141-3910(02)00119-2)
 38. Conesa JA, Caballero JA, Marcilla A and Font R. Analysis of different kinetic models in the dynamic pyrolysis of cellulose. *Thermochimica Acta*. 1995; 254:175-192. [http://dx.doi.org/10.1016/0040-6031\(94\)02102-T](http://dx.doi.org/10.1016/0040-6031(94)02102-T)
 39. Dahiya JB, Kumar K, Muller-Hagedorn M and Bockhorn H. Kinetics of isothermal and non-isothermal degradation of cellulose: model-based and model-free methods. *Polymer International*. 2008; 57:722-729. <http://dx.doi.org/10.1002/pi.2398>
 40. Soares S, Camino G and Levchik S. Comparative study of the thermal decomposition of pure cellulose and pulp paper. *Polymer Degradation and Stability*. 1995; 49:275-283. [http://dx.doi.org/10.1016/0141-3910\(95\)87009-1](http://dx.doi.org/10.1016/0141-3910(95)87009-1)
 41. Scheirs J, Camino G and Tumiatti W. Overview of water evolution during the thermal degradation of cellulose. *European Polymer Journal*. 2001; 37:933-942. [http://dx.doi.org/10.1016/S0014-3057\(00\)00211-1](http://dx.doi.org/10.1016/S0014-3057(00)00211-1)